CORONAVIRUS



# Persistent post–COVID-19 smell loss is associated with immune cell infiltration and altered gene expression in olfactory epithelium

**John B. Finlay[1,2], David H. Brann[3], Ralph Abi Hachem[2], David W. Jang[2], Allison D. Oliva[2], Tiffany Ko[4], Rupali Gupta[2], Sebastian A. Wellford[5], E. Ashley Moseman[5], Sophie S. Jang[6], Carol H. Yan[6], Hiroaki Matsunami[4,7,8], Tatsuya Tsukahara[3], Sandeep Robert Datta[3], Bradley J. Goldstein[2,4]***

**SARS-CoV-2 causes profound changes in the sense of smell, including total smell loss. Although these alterations are often transient, many patients with COVID-19 exhibit olfactory dysfunction that lasts months to years. Although animal and human autopsy studies have suggested mechanisms driving acute anosmia, it remains unclear how SARS-CoV-2 causes persistent smell loss in a subset of patients. To address this question, we analyzed olfactory epithelial samples collected from 24 biopsies, including from nine patients with objectively quantified long-term smell loss after COVID-19. This biopsy-based approach revealed a diffuse infiltrate of T cells expressing interferon-γ and a shift in myeloid cell population composition, including enrichment of CD207$^+$ dendritic cells and depletion of anti-inflammatory M2 macrophages. Despite the absence of detectable SARS-CoV-2 RNA or protein, gene expression in the barrier supporting cells of the olfactory epithelium, termed sustentacular cells, appeared to reflect a response to ongoing inflammatory signaling, which was accompanied by a reduction in the number of olfactory sensory neurons relative to olfactory epithelial sustentacular cells. These findings indicate that T cell–mediated inflammation persists in the olfactory epithelium long after SARS-CoV-2 has been eliminated from the tissue, suggesting a mechanism for long-term post–COVID-19 smell loss.**

## INTRODUCTION

Anosmia, the loss of the sense of smell, occurs in most individuals with coronavirus disease 2019 (COVID-19) but may persist after recovery (*1*–*5*). It is thought that severe acute respiratory syndrome coronavirus 2 (SARS-CoV-2) causes anosmia by affecting the olfactory epithelium, the peripheral organ for olfaction that lines the olfactory cleft of the nasal cavity. The olfactory epithelium houses the primary olfactory sensory neurons responsible for detecting odors, a barrier supporting cell layer composed of sustentacular cells, and a population of basal stem or progenitor cells that continuously renew the olfactory epithelium (*6*–*10*). Commonly, patches of respiratory epithelium are interspersed within the olfactory cleft region and are composed of secretory cells, ciliated cells, and basal cells. Olfactory sensory neurons detect volatile odors via olfactory receptors localized to the neuronal cilia in the nasal airspace (*11*). Transient gene expression changes in olfactory sensory neurons, alterations in the character of the mucus layer surrounding their cilia, and inflammation are thought to cause acute anosmia in animal models of SARS-CoV-2 infection (*12*). Work in both animal models and in human autopsy tissues demonstrates that sustentacular cells rather than neurons are infected by the virus (*13*, *14*). Consistent with sustentacular cells representing a primary site of infection, polymorphisms in the *UGT2A1/UGT2A2* locus, whose gene product is expressed in sustentacular cells, are associated with elevated risk of COVID-19–related acute loss of smell or taste (*15*). It is thought that, in most patients with COVID-19–associated smell loss, after viral clearance the normal epithelial reparative processes reconstitute the sustentacular cell population (and any incidentally damaged neurons), restoring function (*8*).

However, it remains unclear what prevents recovery in the subset of individuals with COVID-19 who have lasting olfactory function loss. There are several non–mutually exclusive possibilities, including severe initial epithelial damage that diminishes or eliminates the basal stem cell pools that normally reconstitute the neuroepithelium. Other possibilities include infiltration of the olfactory epithelium by immune cell populations such that neuroinflammation or autoimmune phenomena perturb normal olfactory function and homeostasis through alterations in gene expression or other means, or central mechanisms that cause derangements in the olfactory bulbs of the brain or olfactory cortex. Examination of human autopsy tissue derived from patients who died from acute sequelae of COVID-19 reveals persistent infection of sustentacular cells, a lack of infection of olfactory sensory neurons, intact epithelial anatomy, and diverse molecular changes in olfactory sensory neurons that could lead to changes in smell detection, although smell was not assessed in any of these patients (*12*, *16*). Whereas these findings suggest mechanisms relevant to acute COVID-19–related loss of smell, to date, there has been no direct examination

[1]Medical Scientist Training Program, Duke University School of Medicine, Durham, NC 27710, USA. [2]Department of Head and Neck Surgery & Communication Sciences, Duke University School of Medicine, Durham, NC 27710, USA. [3]Department of Neurobiology, Harvard Medical School, Boston, MA 02115, USA. [4]Department of Neurobiology, Duke University School of Medicine, Durham, NC 27710, USA. [5]Department of Immunology, Duke University School of Medicine, Durham, NC 27710, USA. [6]Department of Otolaryngology-Head and Neck Surgery, University of California San Diego, San Diego, CA 92037, USA. [7]Department of Molecular Genetics and Microbiology, Duke University School of Medicine, Durham, NC 27710, USA. [8]Duke Institute for Brain Sciences, Duke University School of Medicine, Durham, NC 27710, USA.
*Corresponding author Email: bradley.goldstein@duke.edu

[including single-cell RNA sequencing (scRNA-seq)] of olfactory tissue from humans suffering from long-term olfactory dysfunction, a hallmark symptom of post-acute sequelae of COVID-19 (PASC). Here, we obtained olfactory epithelium biopsies from nine individuals with lasting PASC-related olfactory loss, defined by objective olfactory testing, and used immunohistochemistry and scRNA-seq to identify cellular and transcriptional alterations associated with PASC-related olfactory dysfunction. Controls included newly obtained normosmic olfactory epithelium biopsies, mucus samples, and our published control scRNA-seq datasets for a total of 44 patient samples (tables S1 and S2).

## RESULTS

### Histological assessment of PASC hyposmic olfactory mucosa suggests a role for T cell infiltrates

We performed an initial immunohistochemical assessment of olfactory epithelium biopsies from non-COVID normosmic controls, post-COVID normosmic controls, and nine post–COVID-19 hyposmic individuals, obtained from patients undergoing transnasal endoscopic surgery as described previously (*9*).

Biopsies lacking olfactory epithelium often occur if a disease process has destroyed the olfactory epithelium entirely or if, because of sampling error, the tissue was harvested from an area normally lined by respiratory surface epithelium. In our samples, staining for the neuronal marker TUJ1 confirmed the presence of olfactory neurons, verifying the capture of olfactory epithelium rather than nonsensory respiratory epithelium (Fig. 1A).

Despite our failure to detect SARS-CoV-2 by staining using a validated antibody to the nucleocapsid protein, we observed widespread infiltration of $CD45^+$ immune cells in post–COVID-19 hyposmic mucosa but not in either control group (table S1, Fig. 1A, and fig. S1). Myeloid cells (as assessed by CD68 positivity) appeared similar in PASC hyposmic tissues and normosmic control tissues. T cells, identified by CD3 expression, appeared to be more widespread in PASC hyposmic samples, and many of these were localized within the upper layers of the epithelium itself rather than confined to the deeper stroma as was observed in control tissue (Fig. 1B). We failed to observe cells expressing these same markers in the post–COVID-19 normosmic samples or non–COVID-19 normosmic samples.

### Olfactory biopsy analysis using scRNA-seq

Given the presence of T cell infiltration into the PASC olfactory epithelium, we obtained additional nasal biopsy samples from individuals reporting olfactory dysfunction persisting for at least 4 months since the onset of COVID-19 for analysis by single-cell sequencing (table S1). We preoperatively confirmed hyposmia in these patients using a well-validated smell identification test (*5*, *17*, *18*); many of our COVID-19 patients also subjectively reported some component of parosmia or distorted odor perceptions. Endoscopic olfactory mucosa biopsies were obtained either in the otolaryngology clinic using a surgical or cytology brush technique or in the operating room in patients undergoing unrelated trans-sphenoidal procedures to access the pituitary for benign disease (fig. S2). Sinusitis or other known sinonasal diseases were excluded by endoscopic exam and imaging, ruling out bacterial infection, edema, and polyposis. None of the patients was acutely ill or subject to previous medical interventions, e.g., prolonged intubation.

Biopsies were processed immediately for scRNA-seq analysis, as we have described previously (*9*, *19*). Samples for scRNA-seq included biopsies from six PASC hyposmic individuals (age range, 22 to 58 years; five female and one male, 4 to 16 months after COVID-19 onset). We did not recover transcripts from SARS-CoV-2 in our biopsies, consistent with the absence of ongoing infection or persistent viral RNAemia (*20*, *21*). For comparison, we analyzed three normosmic control samples (age range, 51 to 71 years; two female and one male); to bolster these control data, we combined them with our additional previously published datasets from normosmic and presbyosmic patients to generate an integrated single-cell sequencing dataset from a total of 16 individuals, permitting robust cluster annotation from >124,000 cells (Fig. 1C). Uniform manifold approximation projection (UMAP) plots confirmed that the expected distribution of olfactory, respiratory, and immune cells was captured for analysis.

### Specific T cell subpopulations are enriched in PASC hyposmic olfactory samples

Given our observation of a T cell infiltrate in the olfactory epithelium samples, we asked whether there were any quantitative changes in specific immune cell populations residing in the PASC hyposmic olfactory epithelium. On the basis of the expression of canonical markers (*22*), we were able to identify a wide variety of T cell subtypes present in both the control and PASC hyposmic olfactory epithelium (Fig. 2A). In particular, there was enrichment of resident $CD8^+$ T cells (CD8 $T_{res}$) belonging to cluster 5 (here referred to as CD8 $T_{res}$ 5) (Fig. 2B), which we identified on the basis of immune marker gene expression as γδ T cells (Fig. 2, C and D) (*23*). γδ T cells, found in surface epithelia, exhibit diverse properties with functional specializations dependent on their cytokine production, location, and activation state (*24*). Whereas specific roles for γδ T cells in COVID-19 remain unclear, potential functions in the PASC hyposmic olfactory epithelium may involve protection of epithelial barrier function, tissue remodeling, or an ongoing role in modulating immune responses in the context of severe previous damage and the need for epithelial repair (*23*–*25*).

Of interest, the γδ T cell cluster identified here expresses the inflammatory cytokine interferon-γ (Fig. 2E). Interferon-γ (type II interferon) mediates immunomodulatory responses and adaptive immunity. We did not identify any cell type that expressed type I interferons (interferon-α and interferon-β), which are associated with acute viral infection (fig. S3). Gene expression analysis of sustentacular cells and olfactory sensory neurons revealed expression of receptors for interferon-γ in addition to expression of receptors for a number of other signaling ligands expressed by CD8 $T_{res}$ 5 cells (Fig. 2, F and G). Immunohistochemistry using antibody to γδ T cell receptor confirmed prominent γδ T cell infiltrates in PASC hyposmic olfactory epithelium (fig. S1). These observations demonstrate that the PASC olfactory epithelium harbors a unique population of γδ T cells that express interferon-γ and that both sustentacular cells and olfactory sensory neurons express the relevant cognate receptors to respond to these (and other) inflammation-related ligands.

In a separate cohort of PASC hyposmic samples ($n$ = 13 patients; table S2) and control samples ($n$ = 7 individuals), olfactory mucus was assayed to measure cytokines and chemokines (fig. S4). Consistent with a lack of severe cytotoxic inflammation, there were no markedly elevated changes in interleukin-1β (IL-1β) or tumor necrosis factor–α (TNF-α). Of interest, interferon-λ1 (IFN-λ1), a

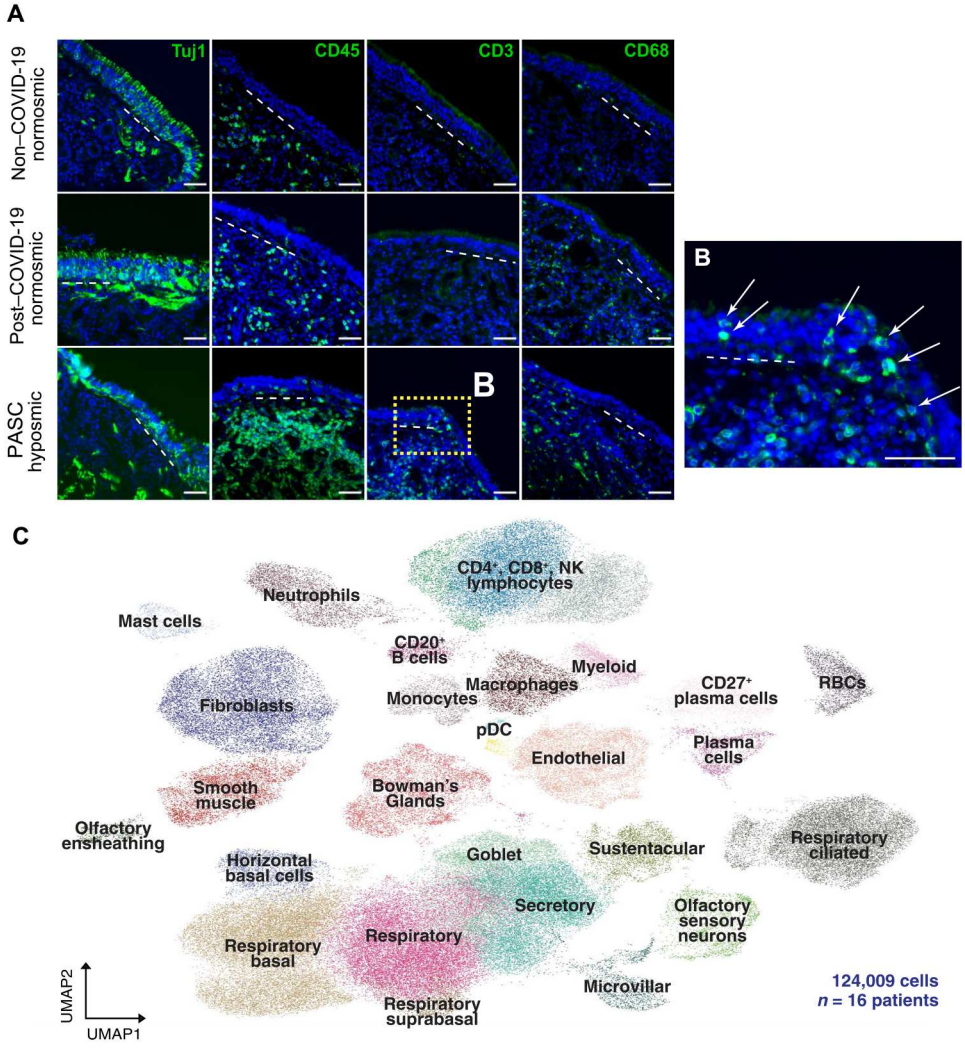


**Fig. 1. T cell infiltrates in nasal olfactory epithelial biopsies from PASC hyposmic patients.** (**A**) Representative immunohistochemistry images of nasal biopsy tissue from normosmic non–COVID-19, normosmic post–COVID-19, or PASC hyposmic individuals. Tissue sections were immunostained for the TUJ1 neuronal marker, CD45 pan-immune cell marker, CD3 T cell marker, and CD68 myeloid cell marker. PASC hyposmic tissue showed dense $CD45^+$ immune cell infiltration, including prominent $CD3^+$ lymphocytic infiltration, which was absent in the normosmic groups; scattered $CD68^+$ cells were present in all conditions. (**B**) Enlarged area (yellow box) from (A) shows $CD3^+$ lymphocytes, with prominent infiltration into the olfactory epithelium (white arrows); dashed white line marks the basal lamina. Scale bar, 50 μm. (**C**) Additional nasal biopsies were processed for scRNA-seq to permit quantitative analyses. Uniform manifold approximation projection (UMAP) visualization of combined PASC hyposmic and control normosmic scRNA-seq datasets integrating 16 human nasal biopsies permitted robust cell cluster analysis and annotation. RBCs, red blood cells; pDC, plasmacytoid DCs.

proinflammatory cytokine, was up-regulated in PASC hyposmic mucus ($P < 0.05$, unpaired $t$ test with Welch's correction). Also, IFN-α2, a type I interferon involved in antiviral immunity, trended toward up-regulation in PASC hyposmic samples ($P = 0.0506$, unpaired $t$ test with Welch's correction). IP-10 (CXCL10), which is directly stimulated by IFN-γ and was observed to be up-regulated at 31 days after infection in a hamster model of olfactory SARS-CoV-2 infection (*21*), was also up-regulated in these samples ($P < 0.05$, unpaired $t$ test with Welch's correction).

### A shift in myeloid cell populations accompanies T cell alterations in PASC hyposmic olfactory epithelium

Given the enrichment of γδ T cells in PASC olfactory epithelium, we focused further attention on the myeloid lineage, which can coordinate alterations in lymphocyte populations. Anti-CD68 staining demonstrated the presence of myeloid cells in both control and PASC olfactory epithelium (Fig. 1A). Analysis of the myeloid clusters by scRNA-seq identified multiple subpopulations, which corresponded to different macrophage, monocyte, and antigen-presenting dendritic cell (DC) subtypes (Fig. 3, A to C). DCs can be segregated on the basis of expression of CD207 (LANGERIN), with the $CD207^+$ population exhibiting enriched expression of CCR6 and Toll-like receptor 10 (TLR10) (Fig. 3, A and C); quantification revealed a shift toward $CD207^+$ DCs in the PASC hyposmic olfactory epithelium, with a corresponding decrease in the $CD207^-$ population (Fig. 3D). Immunostaining confirmed the presence of $CD207^+$ DCs in PASC hyposmic olfactory biopsies (Fig. 3E). Although CD207 is well known for its functional role

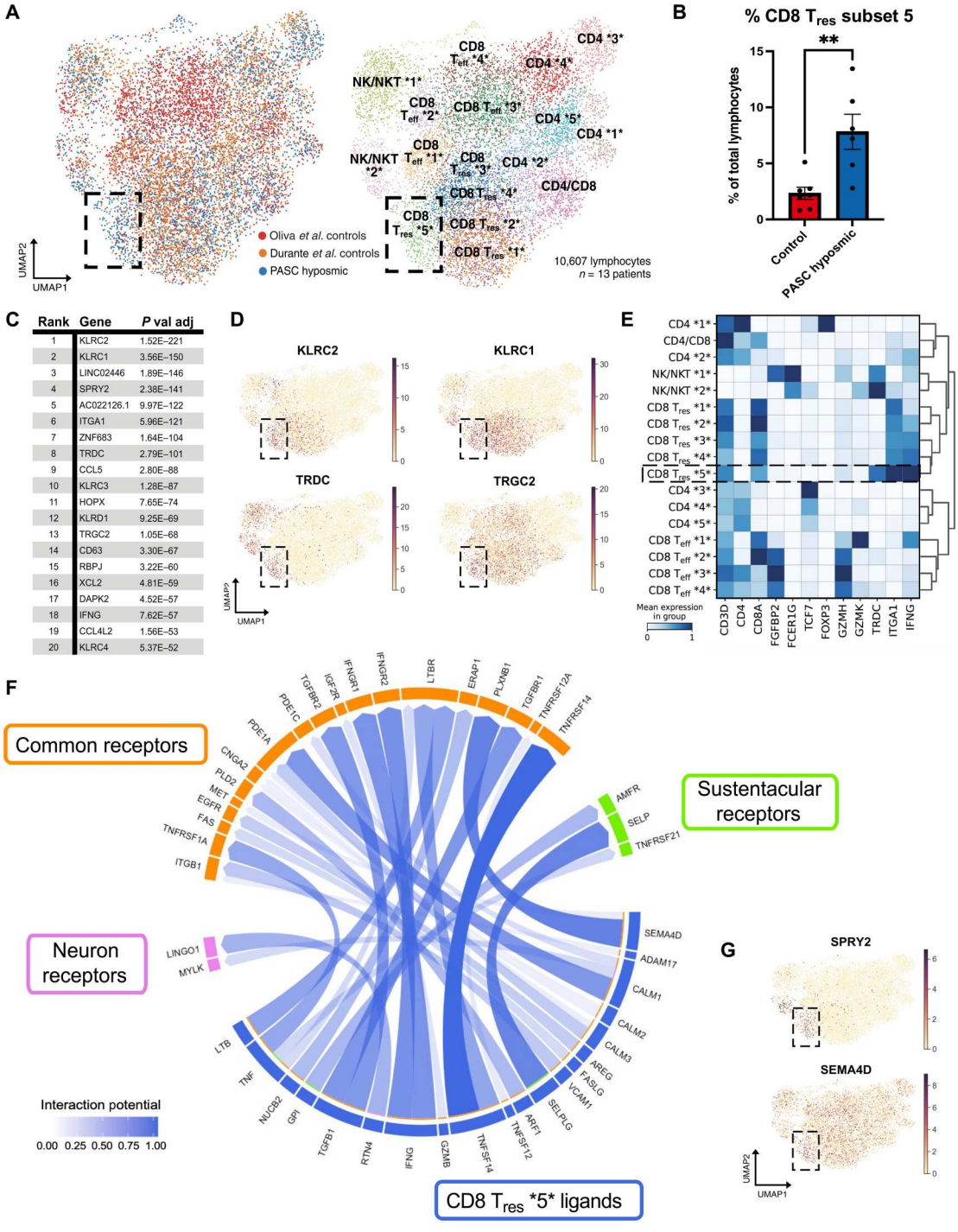


**Fig. 2. A CD8⁺ T cell subset is enriched in nasal olfactory epithelial biopsies from PASC hyposmic patients.** (**A**) UMAP visualization of all lymphocytes from CD8⁺, CD4⁺, and NK/NKT cell clusters in olfactory biopsy scRNA-seq datasets, with comparison of PASC hyposmic datasets to two normosmic control datasets: Oliva *et al.* controls (*19*) were normosmic by smell identification test scores, whereas Durante *et al.* controls (*9*) were normosmic by subjective report. Black box denotes clusters enriched in PASC hyposmic samples. $T_{eff}$, effector T cells; $T_{res}$, resident T cells; subsets within categories are designated by numbers (i.e., CD4 *1* thru CD4 *5*). (**B**) PASC hyposmic biopsies showed enrichment for cell cluster CD8 $T_{res}$ subset 5 compared with both control datasets (two-tailed *t* test, $P = 0.0015$). (**C**) Top-ranked transcripts enriched in CD8 $T_{res}$ subset 5 cluster (by adjusted *P* value, Wilcoxon rank sum test, with Bonferroni correction). (**D**) Selected gene expression plots of significantly enriched genes in the PASC hyposmic-specific cluster CD8 $T_{res}$ subset 5 (black box), including γδ T cell markers and associated genes (TRDC, TRGC2, KLRC1, and KLRC2). (**E**) Selected gene expression and dendrogram clustering among lymphocyte subsets confirming annotations based on published marker genes. The *IFNG* gene is enriched in $T_{res}$ subsets, especially the CD8 $T_{res}$ subset 5. (**F**) Circos plot showing NicheNet analysis of CD8 $T_{res}$-derived ligands and their receptors in either sustentacular cells or olfactory sensory neurons, depicting interaction potential. Common receptors in orange are present in both sustentacular cells and neurons. (**G**) Additional plots confirm that PASC hyposmic γδ T cells express T cell ligands identified by differential gene expression (SPRY2) or NicheNet analysis (SEMA4D).

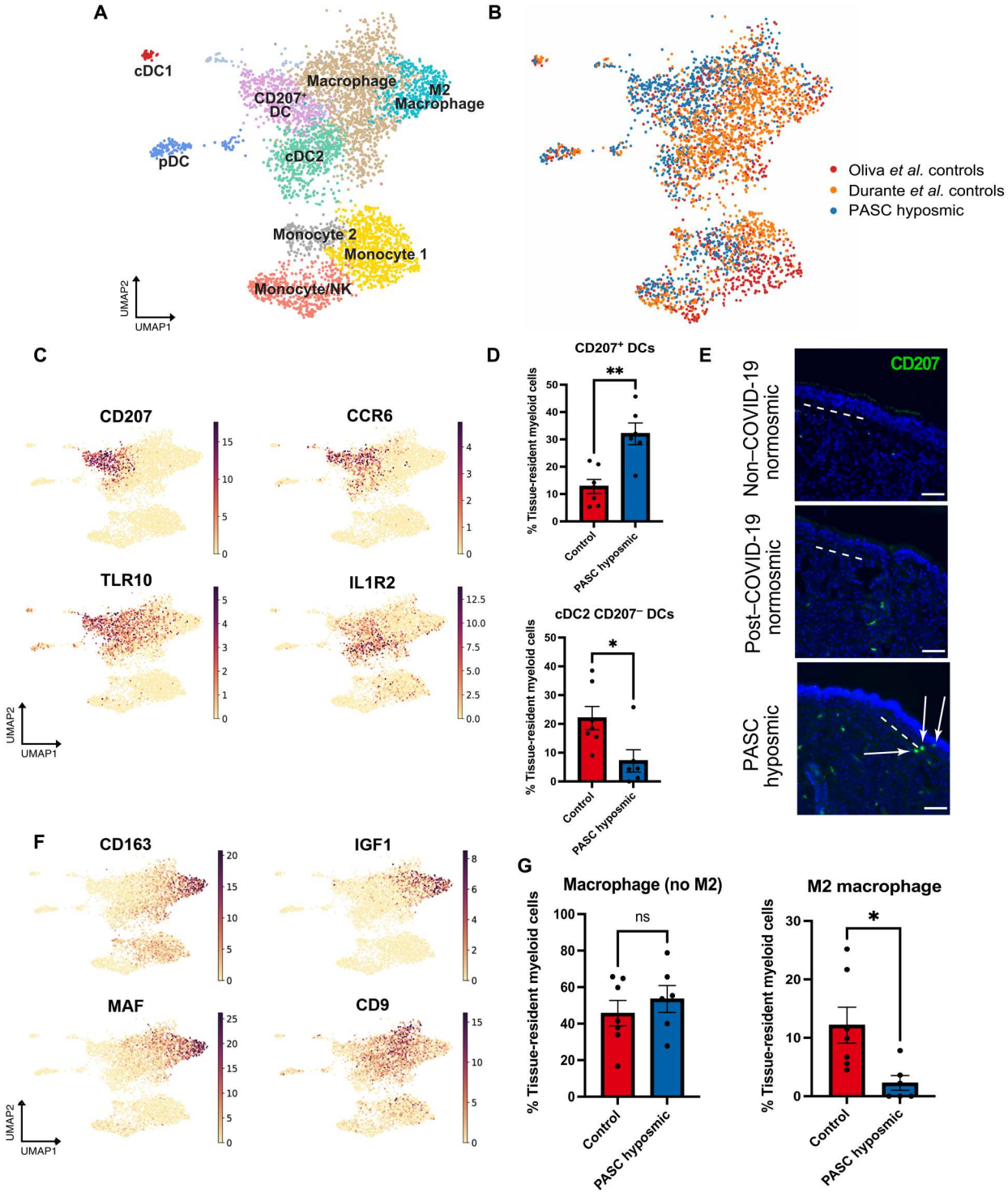


**Fig. 3. PASC hyposmic olfactory epithelial biopsies show a myeloid cell shift with enriched DC subsets and decreased M2 macrophages.** (**A**) UMAP visualization of olfactory biopsy scRNA-seq data for selected myeloid cell clusters, comparing PASC hyposmic to both normosmic control datasets (*9*, *19*). DC, dendritic cells; pDC, plasmacytoid DCs (CLEC4C$^+$); cDC1, conventional DC type 1 cells (CLEC9A$^+$); cDC2, conventional DC type 2 cells (CLEC10A$^+$). (**B**) UMAP plots in (A), colored by sample contribution. (**C**) Selected gene expression plots confirm cluster annotation for CD207$^+$ DCs and additional marker genes obtained by differential gene expression analysis for the CD207$^+$ DC cluster (CCR6 and TLR10) and the cDC2 cluster (IL1R2). (**D**) CD207$^+$ DCs are enriched in PASC hyposmic biopsies (blue) compared with normosmic control biopsies (red) (two-tailed *t* test, $P = 0.0016$; CD207$^-$ DCs are reduced, $P = 0.0236$). (**E**) Anti-CD207 antibody staining confirmed CD207$^+$ dendritic cells in PASC hyposmic nasal biopsies (white arrows); dashed white lines mark the basal lamina. Scale bar, 50 μm. (**F**) Gene expression plots indicate marker genes for M2 macrophage (CD163, MAF, and IGF1) and total macrophage (CD9) clusters. (**G**) PASC hyposmic biopsies showed depletion of M2 macrophages relative to all resident myeloid cells (two-tailed *t* test, $P = 0.0175$).

within skin Langerhans cells, CD207$^+$ DCs are broadly distributed and are thought to survey tissues and coordinate immune responses, including T cell activation (*26*, *27*). TLR10, a protein enriched in CD207$^+$ DCs, plays a role in myeloid cell detection of influenza virus and subsequent organization of the immune response (*28*). Thus, the enrichment of CD207$^+$ DC cells may help to orchestrate the immune infiltration seen in PASC hyposmic olfactory epithelium samples.

Analysis of macrophage clusters revealed a distinct population of anti-inflammatory M2 macrophages marked by CD163 (Fig. 3, A and F). Whereas there was no difference in the relative numbers of CD163$^-$ macrophages, we observed significantly fewer M2 macrophages in PASC hyposmic olfactory epithelium (Fig. 3G; $P = 0.0175$, two-tailed $t$ test). A reduction in M2 macrophages is of interest because this population can promote tissue repair via several mechanisms, especially given that the M2 macrophage population observed here produces insulin-like growth factor 1 (IGF1), a known growth factor for olfactory sensory neurons (*29*, *30*). This relative reduction in the M2 macrophages in the PASC hyposmic olfactory epithelium might also serve as a readout for the presence of ongoing proinflammatory signaling, biasing macrophages away from the M2 identity.

### Sustentacular cells exhibit an immune response phenotype in PASC hyposmic olfactory samples

Sustentacular cells express coronavirus entry genes, and SARS-CoV-2 has been found to infect this cell population during acute COVID-19 (*12*–*14*). Sustentacular cells have multiple functions as the apical barrier cell lining the olfactory epithelium, including detoxification of harmful chemicals via robust expression of biotransformation enzymes, modulation of the ion content of the mucus layer in which olfactory sensory neuron cilia are embedded, and feedback regulation of olfactory epithelium neuronal stem cells (*31*, *32*). On the basis of expression of canonical sustentacular markers such as ERMN (*9*), CYP2A13, and GPX6, we identified 779 high-quality sustentacular cells from PASC hyposmic or control samples (Fig. 4A). We observed strong expression in sustentacular cells of *UGT2A1*, a gene shown by genome-wide association study to convey elevated risk of olfactory loss in COVID-19 (*15*).

Differential gene expression analysis identified marked transcriptional alterations between PASC hyposmic and control sustentacular cells (Fig. 4B and fig. S5). Consistent with sustentacular cells mounting a response to inflammation, antigen presentation genes were enriched in sustentacular cells derived from PASC hyposmic samples (Fig. 4C and fig. S5, B to D), with minimal changes in typical markers of active viral infection such as CXCL10, PTX3, or CD46. Consistent with the absence of acute viral responses, we did not detect SARS-CoV-2 transcripts in scRNA-seq biopsy samples from PASC hyposmic patients aligned to the viral reference genome. Gene set enrichment analysis of the transcripts significantly up-regulated in PASC hyposmic samples ($\log_2$ fold change $> 0.6$, $P < 0.05$) identified several biological processes including interferon signaling and antigen presentation (Fig. 4D). Together, these findings suggest that sustentacular cells do not remain infected with SARS-CoV-2 during PASC but rather appear to be responding to local proinflammatory cytokines in their microenvironment.

Previous bulk RNA-seq analysis of hamster olfactory epithelium after SARS-CoV-2 infection identified a set of pathogen response genes that were up- or down-regulated 1 month after infection of sustentacular cells and other cell types (Fig. 4E) (*21*). We therefore asked whether these same genes were altered in our human PASC olfactory epithelium samples obtained 4 months or more after initial infection. Of the pathogenic response genes identified in hamsters, only BST2 was significantly enriched (adjusted $P$ value $< 0.05$, Wilcoxon rank sum test). BST2 (also known as Tetherin) is an interferon-induced host gene encoding a transmembrane protein with antiviral and inflammatory signaling activities (*33*, *34*). We performed identical analysis on all other olfactory epithelium cell populations, which revealed significant changes only in BST2 expression specifically in horizontal basal cells (fig. S6; $P < 0.05$, Wilcoxon rank sum test). Consistent with the absence of viral RNA in post–COVID-19 hyposmic olfactory epithelium samples, we observed no significant increase in any olfactory epithelium cell populations of ISG15, whose expression correlates with the presence of subgenomic nucleocapsid SARS-CoV-2 RNA (*21*).

We validated these findings through immunohistochemical staining of non–COVID-19 normosmic, post–COVID-19 normosmic, and PASC hyposmic biopsies (Fig. 4F). Anti-ERMN, which selectively labels the apical region of sustentacular cells but not respiratory epithelial cells, exhibited a strong uniform signal in both sets of control biopsies and in PASC hyposmic biopsies (Fig. 4F). In contrast, TUJ1 antibody, which stains immature olfactory sensory neuron somata and neurites, exhibited abundant labeling in the control samples but less consistent labeling in PASC hyposmic samples (Fig. 4F and fig. S7).

### The olfactory neuron population is reduced in PASC hyposmic samples

Despite the lymphocytic infiltrates in PASC hyposmic samples, pseudotime analysis confirmed the expected olfactory epithelium lineage relationships and marker gene expression within the olfactory epithelium, an adult neurogenic niche (Fig. 5, A and B). Further analysis of the neuronal lineage subsets identified globose basal cells/neuronal precursors, immature olfactory sensory neurons, and mature olfactory sensory neurons, suggesting that olfactory epithelium neurogenesis capacity was not exhausted in the PASC hyposmic samples (Fig. 5, C and D). However, analysis of PASC hyposmic horizontal basal cells, which can express the SARS-CoV-2 receptor ACE2, revealed down-regulation of subsets of transcripts involved in epithelial renewal (fig. S8), in line with observed horizontal basal cell changes in mouse models of localized inflammatory exposure (*35*). Analysis of olfactory sensory neuron–specific genes suggested modest alterations in PASC hyposmic samples. For instance, expression of signaling factors downstream of their olfactory receptors was broadly similar between PASC hyposmic and control groups (Fig. 5E; adjusted $P$ value not significant, Wilcoxon rank sum test). To quantify the number of olfactory sensory neurons on the basis of the scRNA-seq data, we normalized olfactory sensory neuron counts to sustentacular cell counts (Fig. 5F; $n = 5$ PASC hyposmic, $n = 5$ controls; $P = 0.034$, two-tailed $t$ test). We used this approach because olfactory epithelium biopsies can be variable and because there are often patches of respiratory-like metaplasia in biopsies. When normalized in this manner, the number of olfactory sensory neurons was reduced relative to sustentacular cells in the PASC hyposmic samples compared with control samples. However, despite the reduction in olfactory sensory neuron number, we observed no differences in the frequency of cells expressing olfactory receptors, the mRNA expression of

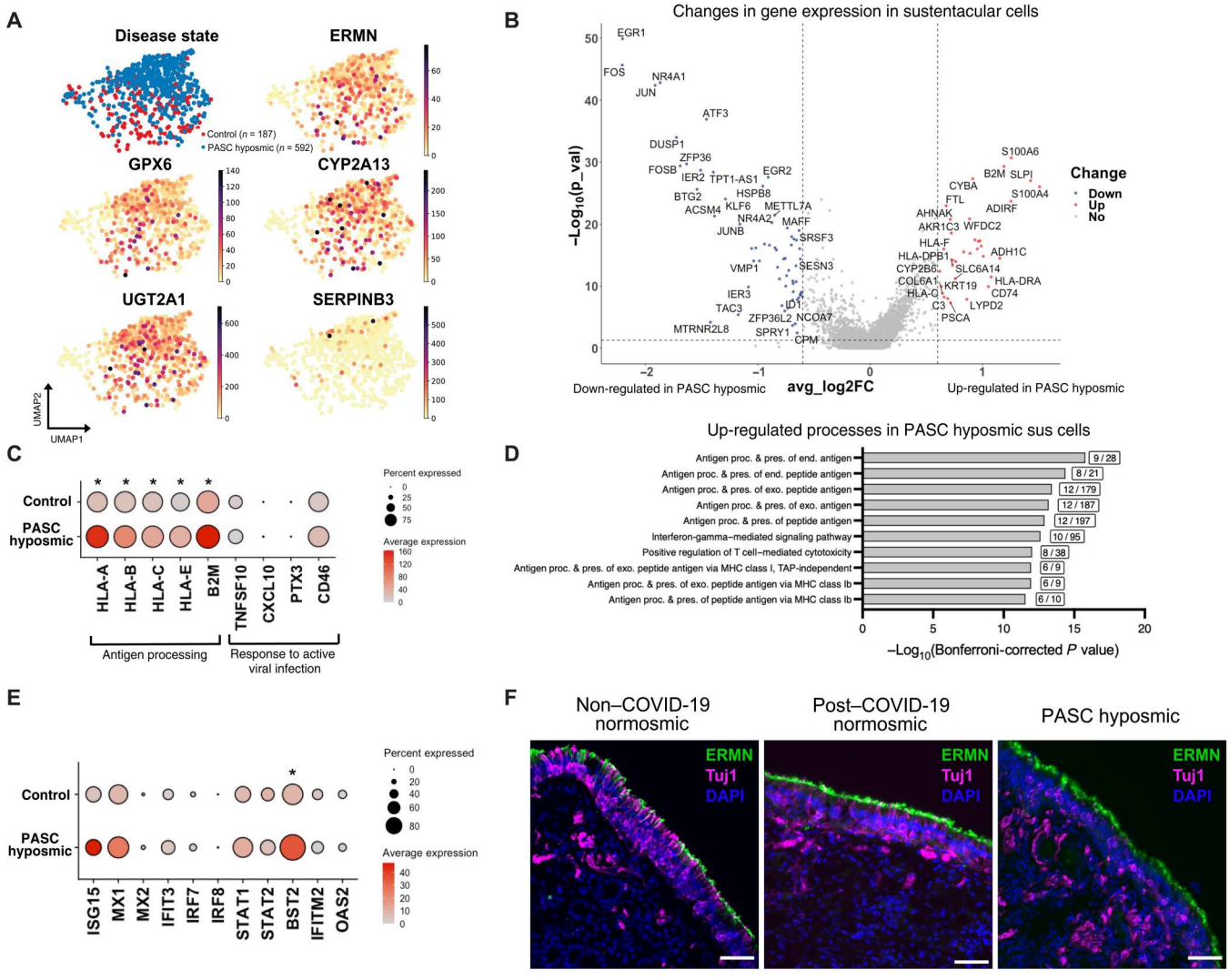


**Fig. 4. Sustentacular cell gene expression changes persist in PASC hyposmic olfactory epithelium.** (**A**) UMAP visualization of sustentacular cell subsets in olfactory biopsy scRNA-seq datasets from PASC hyposmic samples (blue) and normosomic control samples (red) ($n$ = 9 nasal biopsies: 6 PASC hyposmic, 3 normosmic). Gene expression plots show expression of selected canonical sustentacular cell markers (ERMN, GPX6, and CYP2A13) and minimal expression of the respiratory marker SERPINB3. (**B**) Volcano plot showing differential gene expression in sustentacular cells in PASC hyposmic and normosmic control olfactory epithelial biopsies; red or blue indicates significant change of >0.6 $\log_2$ fold change, $P < 0.05$. (**C**) Visualization of expression of selected antigen presentation genes and genes normally involved in responses to active viral infection in sustentacular cells in PASC hyposmic and normosmic control samples (antigen presentation genes were significantly up-regulated in PASC hyposmic samples, with adjusted $^*P < 0.05$ by Wilcoxon rank sum test). (**D**) Gene set enrichment analysis of the transcripts up-regulated in PASC hyposmic sustentacular (sus) cells in (C) identifies a variety of biological processes, including antigen presentation and IFN-γ signaling. Boxes show number of altered genes per process term; only significant processes are included based on $-\log_{10}$(Bonferroni-corrected $P$ value). (**E**) Differential gene expression of pathogen response genes previously identified in sustentacular cells in hamsters 31 days after SARS-CoV-2 infection or in uninfected animals (*21*). BST2, an interferon-induced host gene encoding a transmembrane protein with antiviral and inflammatory signaling activities, adjusted $P < 0.05$; STAT1, a transcription factor downstream of inflammatory signaling, adjusted $P < 0.1$, Wilcoxon rank sum; see also fig. S5; $^*P < 0.05$. (**F**) Representative images of immunohistochemical staining of the sustentacular cell marker ERMN (green) and the neuronal marker TUJ1 (magenta) in PASC hyposmic and normosmic control biopsies. Nuclei are stained with DAPI (blue). Scale bar, 50 μm.

olfactory receptor genes, or the distribution of olfactory receptors expressed across olfactory sensory neurons (fig. S9). In contrast to widespread marked olfactory sensory neuron gene expression changes reported in human autopsy samples after fatal acute COVID-19 (*12*), the PASC hyposmic olfactory sensory neuron changes identified here were limited (Fig. 5E and fig. S9).

To further validate the reduction in olfactory sensory neuron numbers identified by scRNA-seq, we performed immunohistochemical staining on additional samples, including non–COVID-19 normosmic ($n$ = 3), post–COVID-19 normosmic ($n$ = 2), and PASC hyposmic ($n$ = 3) biopsies. We visualized mature olfactory sensory neurons with anti–olfactory marker protein (OMP) antibody (*36*–*38*) and sustentacular cells with apical layer anti-SOX2 antibody (Fig. 5G and fig. S7) (*9*, *38*). In both non–COVID-19 and post–COVID-19 normosmic groups, we identified prominent OMP$^+$ neurons and well-organized

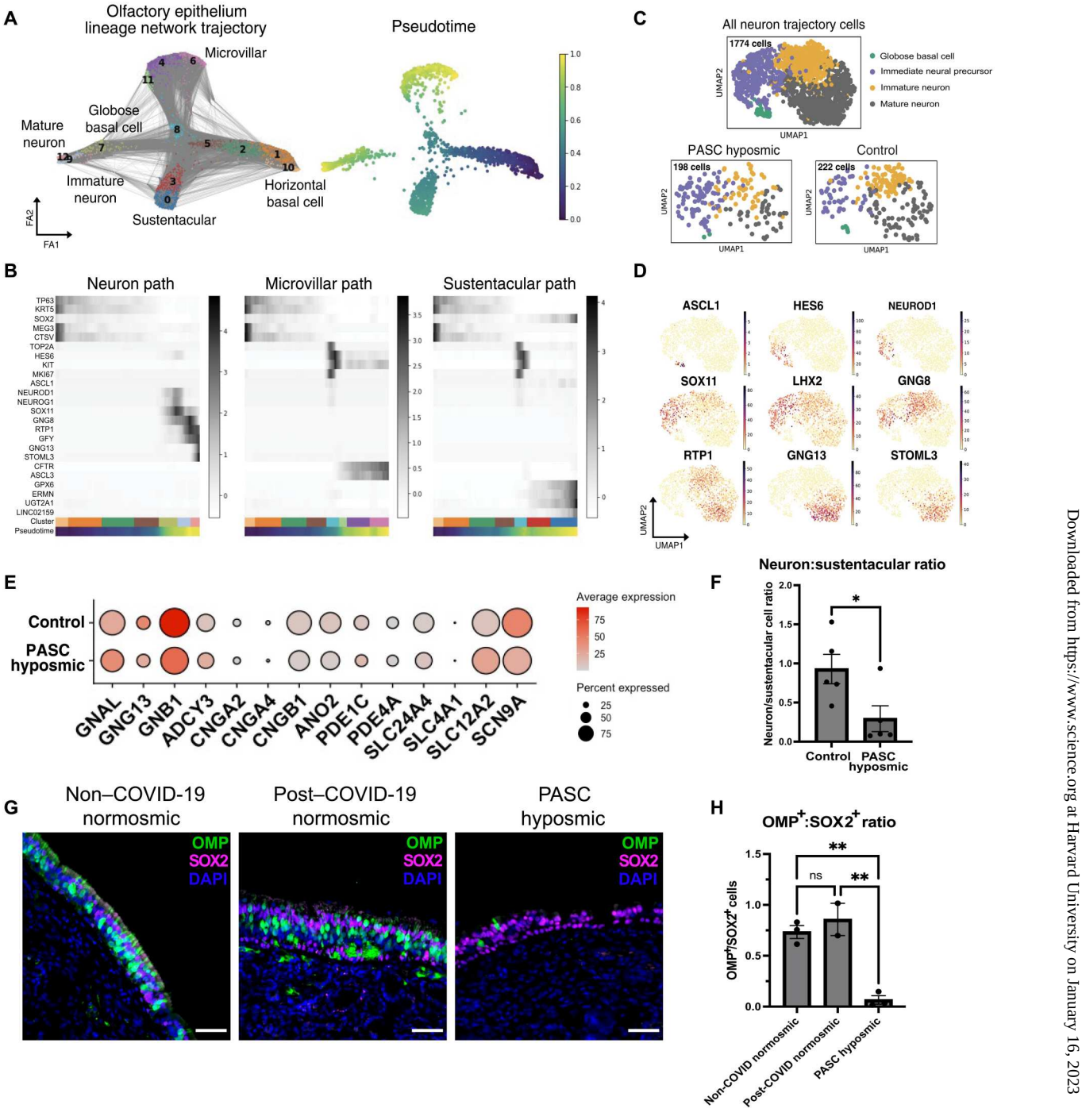


**Fig. 5. Analysis of olfactory sensory neurons in PASC hyposmic nasal biopsies.** (**A**) Trajectory lineage analysis of cells in olfactory epithelium in PASC hyposmic biopsies ($n$ = 4) compared with normosmic control biopsies ($n$ = 3). Cells include horizontal basal cells, globose basal cells, olfactory sensory neurons, sustentacular cells, and microvillar cells. (**B**) Heatmaps showing pseudotime progression for olfactory epithelial cell lineages labeled on the basis of UMAP relations in (A). Representative transcript markers for each cellular differentiation state are shown on the $y$ axis. (**C**) UMAP visualization showing annotations within the olfactory sensory neuron cluster from Fig. 1D. "All neuron trajectory cells" includes neuron lineage cells in five PASC hyposmic biopsies and three normosmic control biopsies. (**D**) Gene expression plots show established markers of the olfactory sensory neuron differentiation pathway. (**E**) Selected gene expression in olfactory sensory neurons (mature and immature) in PASC hyposmic compared with normosmic control biopsies. (**F**) Ratio of olfactory sensory neurons (mature and immature) to sustentacular cells in PASC hyposmic ($n$ = 5) compared with normosmic control ($n$ = 5) biopsies. Error bars indicate SEM; two-tailed $t$ test, $P$ = 0.034. (**G** and **H**) Immunohistochemistry confirmed a reduction in mature olfactory sensory neurons labeled with an anti-OMP antibody in PASC hyposmic biopsies. Sustentacular cells were labeled with an anti-SOX2 antibody; nuclei are stained with DAPI (blue). $P$ < 0.01, one-way ANOVA with Tukey test and Bonferroni correction.

SOX2$^+$ apical sustentacular cell nuclei. In contrast, PASC hyposmic biopsies contained sparse OMP$^+$ neurons, and the ratio of mature olfactory sensory neurons to sustentacular cells was significantly reduced [Fig. 5, G and H; $P < 0.01$, one-way analysis of variance (ANOVA) with Tukey test and Bonferroni correction]. There was no difference in the OMP$^+$ neuron population in non–COVID-19 normosmic versus post–COVID-19 normosmic samples. We verified that our analysis was performed on regions containing olfactory epithelium rather than respiratory metaplasia on the basis of the presence of cells positive for the sustentacular-specific marker ERMN and for the immature neuronal marker TUJ1 (fig. S7). These findings suggest a model in which immune infiltration, together with changes in stem cell and sustentacular cell function, converges to alter the number of mature olfactory sensory neurons, leading to persistent loss of smell.

## DISCUSSION

SARS-CoV-2 infection can cause persistent dysfunction across many physiological systems, although the mechanisms that distinguish PASC from more acute pathophysiology remain to be determined (*39*, *40*). Current evidence for COVID-19 damage within the human olfactory epithelium comes largely from autopsy studies involving patients who died from severe acute COVID-19; these studies lacked objective measurements of smell, and samples were obtained after major medical intervention (*12*, *16*). Here, we provide an analysis of olfactory tissue biopsies from COVID-19 patients with PASC hyposmia, each of whom exhibited olfactory dysfunction after COVID-19 as documented by objective testing. Our results comparing scRNA-seq data between endoscopically guided olfactory epithelium biopsies from PASC hyposmic patients and control normosmic individuals suggest a model in which altered interactions between immune cells and olfactory epithelium drive functional changes in sustentacular cells and olfactory sensory neurons.

Our findings are consistent with indolent localized immune cell responses driving phenotypic changes in sustentacular cells and olfactory sensory neurons. The changes observed in olfactory sensory neurons, including a relative reduction in cell number, especially of mature OMP$^+$ neurons, could explain sensory dysfunction including hyposmia or parosmia. The absence of marked olfactory sensory neuron transcriptomic changes that we observed in the context of PASC-related hyposmia suggest some differences from findings in autopsy samples from acute COVID-19 cases (*12*). Acutely, local nonautonomous signals are thought to drive neuronal gene expression changes in the setting of severe inflammation. In PASC hyposmic olfactory epithelium, severe inflammation appears absent, and we instead identify interferon response signatures in the sustentacular cells, along with the presence of local lymphocyte populations expressing IFN-γ and γδ T cell markers, unique to the PASC hyposmic olfactory epithelium samples.

It is interesting to compare the phenotypes observed in humans with PASC-related smell loss and those observed previously in hamsters acutely infected with SARS-CoV-2 (*12*, *14*). In the hamster model, a wide array of immune cells (including macrophages, neutrophils, and monocytes) infiltrates the epithelium in the first several days after infection before resolving nearly completely within 2 weeks. Our observation of a persistent infiltration of T cells in the human olfactory epithelium months after SARS-CoV-2 infection suggests that COVID-19 patients with PASC hyposmia may have a selective immunological response to previous infection that differs from the immunological responses generated acutely.

Our data are consistent with a provisional model in which a dysregulated axis among immune cells, horizontal basal cells, sustentacular cells, and olfactory sensory neurons arises in the PASC hyposmic olfactory epithelium, with a resultant sensory dysfunction. How and why this occurs in a subset of patients remain to be determined, but analysis of macrophages from patients with COVID-19 has shown that acute SARS-CoV-2 infection drives a proinflammatory reprogramming that is thought to induce long-term alterations in the function of other immune cells (*41*). In addition, in mouse models (*35*) and in presbyosmic humans (*19*), horizontal basal cells exhibit immune-responsive phenotypes, including signaling interactions that can recruit additional immune cells. Furthermore, unresolved immune responses, including activation of specific CD8$^+$ T cell clonotypes during convalescence after SARS-CoV-2 infection, have been reported (*42*). It is tempting to speculate that these or similar processes may initiate the local olfactory epithelium immune cell alterations identified in our PASC hyposmic samples.

The data presented here are also relevant to several alternative mechanistic hypotheses about how SARS-CoV-2 infection might cause long-term olfactory loss. One possibility suggested by work in animal models is that severe initial widespread cell damage might overwhelm the capacity of basal stem cells to reconstitute the olfactory epithelium, but our samples suggest that many areas of the human olfactory cleft harbor intact olfactory epithelium composed of olfactory sensory neurons, sustentacular cells, and basal cells (*14*). Persistent viral infection could also drive ongoing damage (*43*), but we find no evidence for active SARS-CoV-2 infection in our samples. Another possibility is that anosmia/parosmia is the consequence of severe ongoing mucosal inflammation, but our patients did not exhibit clinical inflammatory findings of local edema, polyposis, or infection, and the molecular signatures identified in the olfactory epithelium were not consistent with broad inflammatory responses. Notably, central mechanisms may contribute to PASC-related smell loss, warranting further study. However, there is little evidence for SARS-CoV-2 infection of neurons in humans (*16*), and at least some of the observed imaging changes in the olfactory bulb or cortex (*44*) could reflect reduced peripheral input due to olfactory epithelium damage (the clear site of viral infection) or diffusion of inflammatory intermediates across the cribriform plate.

There are several limitations associated with our study. Given challenges related to the pandemic, it has been difficult to obtain samples from large numbers of patients with COVID-19, and thus, our conclusions are driven by findings we observed in common across our limited set of patient samples. Furthermore, in our study, we merged patient samples obtained by two different methods, surgical excision and brush biopsy (fig. S10). We did not identify batch effects or gene expression changes related to biopsy technique (fig. S11). Last, although we were careful to obtain biopsies from within the olfactory cleft region, the possibility of sample-to-sample variation in the specific contents of each olfactory epithelium biopsy was unavoidable.

The pandemic has highlighted the unmet need for new effective treatments for olfactory loss. The mechanistic insights provided here suggest potential new therapeutic strategies. For instance,

selectively blocking local proinflammatory immune cells or directly inhibiting specific signaling nodes may interfere with a loop disrupting olfactory epithelium homeostasis or repair. The location of the olfactory epithelium, lining the olfactory cleft in the nose, is amenable to localized topical drug delivery, which may provide a means to avoid systemic or off-target effects of new therapeutic agents. Further studies testing therapeutics in animal models and humans, and longer follow-up of patients with PASC olfactory dysfunction, will provide ongoing insights regarding the etiology and management of olfactory sensory dysfunction.

## MATERIALS AND METHODS

### Study design

We performed a prospective analysis of olfactory epithelial biopsy tissue obtained from nine patients with post–COVID-19 hyposmia/anosmia. Olfactory function was measured using the Smell Identification Test (Sensonics Inc.). Biopsy samples were collected for either histology or scRNA-seq analysis. Patient demographics, including length of hyposmia/anosmia and time since acute COVID-19 infection, were collected (table S1). Control samples included olfactory tissue biopsies obtained from normosmic individuals with no history of COVID-19 (three people) and from normosmic individuals who had been previously diagnosed with COVID-19 (two patients). All human studies were performed under protocols approved by the Institutional Review Boards of Duke University and University of California San Diego.

### Biopsy collection and processing

All biopsy samples reported here were collected under Duke University School of Medicine Institutional Review Board protocols 00088414 and 00105837. Patients were administered the Smell Identification Test before tissue collection to assess olfactory function. For surgical biopsies, olfactory mucosa was collected either in the operating room in patients undergoing transsphenoidal surgery for resection of a benign pituitary tumor or in the clinic. Briefly, using endoscopic visualization, olfactory cleft mucosa was sharply incised, elevated from underlying bone, and then excised with a through-cutting ethmoid forceps. For nasal cytology brush biopsies, tissue was collected in the clinic by gently positioning a cytology brush (catalog no. 4290, Hobbs Medical Inc., Stafford Springs, CT) in the olfactory cleft under endoscopic visualization (fig. S10). The brush was rotated briefly to collect surface mucosal cells. In all cases, samples were placed into collection solution [Hanks′ balanced salt solution (HBSS) or Hibernate-E medium, with 10% fetal bovine serum (FBS; all from Thermo Fisher Scientific, Waltham, MA)] on ice and processed immediately for analysis.

Surgical biopsy tissues were divided into smaller pieces sharply. All biopsies were digested for 15 min at 37°C with an enzyme cocktail composed of dispase/collagenase A/EDTA mix, papain (2 mg/ml), and deoxyribonuclease I (all from STEMCELL Technologies, Vancouver, BC, Canada) with frequent gentle trituration. After 15 min, Accutase (STEMCELL Technologies) was added, and samples were incubated for an additional 5 min at 37°C. At the end of 5 min, FBS was added. If samples still contained large pieces of tissue, they were filtered through a 250-μm filter. All samples were then filtered through a 70-μm filter and centrifuged for 5 min at 400*g*. If abundant red blood cells were observed in the pellet, tissues were resuspended in ACK Lysing Buffer (Thermo Fisher Scientific) and incubated at room temperature for 3 to 5 min with gentle rocking. Samples were washed, spun, and resuspended in HBSS or Hibernate-E containing nonacetylated bovine serum albumin (1 mg/ml; Thermo Fisher Scientific), anti-clumping reagent (0.5 μl/ml; Gibco), and *N*-acetyl cysteine (5 μg/ml; Sigma-Aldrich, St. Louis, MO) to a final concentration of 1 million cells/ml. Brush biopsies were processed similarly but required slightly less time in dissociation enzymes and did not require an erythrocyte lysis step.

### Single-cell sequencing

Samples were processed for single-cell analysis as described previously (*19*). Briefly, cells were quantified with a viability stain on an automated counter (Cellaca MX, Nexcelom) and loaded onto a Chromium controller (10X Genomics, Pleasanton, CA) for cell capture and bar coding targeting 10,000 cells, per the 3′ v3.1 gene expression protocol per the manufacturer′s instructions. Reverse transcription, amplification, library preparation, and sequencing (NovaSeq, Illumina) were performed per protocol.

### Single-cell RNA-seq analysis

Illumina base call files were converted to FASTQ files and processed through CellRanger Counts 6.1.2 (10X Genomics), aligned to either a human reference genome (GRCh38) or a combined reference genome containing human and SARS-CoV-2 genomes (*45*). Starting from the raw cell by gene count matrices, data integration and preprocessing were performed using Scanpy (v1.8.2) and scvi-tools (v0.15.2). For accurate cell type identification, the data generated in this study were combined with our published human olfactory datasets (GSE139522, GSE184117) (*9*, *19*). Highly variable genes (HVGs) were identified using the scvi-tools "poisson_gene_selection" function (with patient ID as the batch key), and the raw counts for these gene subsets were used as the input to the variational autoencoder (scVI) model. An scVI model (using the top 3000 HVGs) was trained for 500 unsupervised epochs with the default learning rate (with early stopping when the ELBO validation metric did not improve for at least 20 epochs) with the default parameters (10 latent dimensions and 128 nodes per hidden layer), a negative binomial observation model (gene_likelihood = "nb"), the percentage of mitochondrial genes as a continuous covariate, and categorical covariate keys for the patient condition and patient ID categorical variables (which thus performed dataset integration and batch correction for the purposes of cell type identification). A *k*-nearest neighbor graph was constructed from the resulting 10-dimensional latent embedding (using $k = 15$ neighbors). The knn graph was used for cell type clustering via the Leiden algorithm (resolution = 1.2) and as the input to the UMAP algorithm (with min_dist = 0.5) for visualization. Clusters of dying cells containing high percentages of mitochondrial genes and low total counts as well as a cluster of cell doublets were removed, and the above procedure starting from the HVG identification was repeated (but with Leiden clustering resolution = 1.6). The resulting cell type clusters were merged and manually annotated on the basis of known cell type markers.

After identifying and annotating the broad clusters, we further subcultured cell types of interest in an iterative manner using the same scVI embedding approach, starting from the reidentification of HVGs for each subset. After training an scVI model using only cell types in the olfactory epithelium (including olfactory horizontal

basal cells, sustentacular cells, Bowman's gland cells, microvillar cells, and olfactory sensory neurons), we identified and removed an additional cluster of olfactory sensory neuron–sustentacular cell doublets. Next, an scVI model was trained on the olfactory sensory neurons and microvillar cells (except using 2000 HVGs and 100 hidden nodes in the scVI model), and the resulting clusters from this model identified cell types of the olfactory sensory neuron lineage; a final scVI model (using 2000 HVGs and 100 hidden nodes) was used to embed and cluster these cells, and the olfactory sensory neuron lineage cell types were manually annotated using known markers for globose basal cells (TOP2A and ASCL1), immediate neuron precursors (NEUROD1 and SOX11), immature olfactory sensory neurons (GAP43, DCX, and GNG8), and mature olfactory sensory neurons (GNG13 and STOML3). The same approach was also used to further subcluster the broad lymphocyte cluster that contained the $CD4^+$ T cells, $CD8^+$ T cells, and natural killer (NK) cells starting from the top 2000 HVGs from these cells, and the resulting scVI embedding was then clustered (resolution = 1.1) to identify the lymphocyte subtypes.

Trajectory and pseudotime analyses were performed using olfactory sensory neuron lineage cell types identified in the second iteration of the scVI model trained on these cells. Bowman's gland cells were excluded from analysis. A new neighborhood graph was computed using n_neighbors = 100 and n_pcs = 20, and cells were reclustered using the default Leiden algorithm with resolution = 1.5. Cluster connectivity was then calculated using partition-based graph abstraction (PAGA) with default settings. PAGA plots were constructed using threshold = 0.2. For plotting of pseudotime heatmaps, Leiden clusters were ordered on the basis of PAGA connectivity predictions.

Transcriptome distances were calculated from the pairwise correlation distance matrix of the embedding in the 10-dimensional scVI latent space embedding for cells from the olfactory sensory neuron lineage. Transcriptome distances were summarized for each olfactory sensory neuron cluster–condition (control versus PASC hyposmic) pair by taking the median pairwise transcriptome distance between cells of each pair.

For additional plots, such as differential expression analysis, filtered outputs were analyzed in R (v4.1.1) using the Seurat toolkit (v4.1.0) (*46*). Processed anndata objects from Scanpy were converted to R objects preserving all metadata (including scVI clusters) using the LoadH5Seurat function from SeuratDisk. Data were normalized using relative counts normalization before differential expression analysis. Differentially expressed genes were found using the FindMarkers function with default settings (Wilcoxon rank sum) and plotted using ggplot2 (identifying significant differentially expressed genes with $>\log_2$ fold change, adjusted $P < 0.05$). Cluster markers of lymphocyte subsets were identified using FindAllMarkers with default settings. DotPlots were produced using relative normalized counts.

NicheNet analysis was conducted in R with the nichenetr package (v.1.1.0) using the default ligand-target previous model, ligand receptor network, and weight integrated networks (*47*). Specifically, cell populations of interest (i.e., lymphocyte clusters, olfactory sensory neurons, and sustentacular cells) with normalized gene expression were subset out from processed R objects (from anndata) and used as input for the appropriate receiver and sender populations. Circos plots were generated using Circlize (v.0.4.14). We analyzed datasets from only-surgical or only-brush biopsy samples for individual comparisons (fig. S11), verifying no significant changes in the normalized olfactory epithelium cell population gene expression profiles.

### Immunohistochemistry

Samples for histology were collected in HBSS (Gibco) + 10% FBS. Tissues were fixed with 4% paraformaldehyde (Sigma-Aldrich, St. Louis) in phosphate-buffered saline (PBS) for 4 hours at room temperature. Samples were washed with PBS and then incubated on a rocker at 4°C for 5 to 7 days in 30% sucrose, 250 mM EDTA, and PBS. Samples were then flash-frozen in Optimal Cutting Temperature compound (VWR, Radnor, PA), sectioned at 10 μm on a cryostat (CryoStar NX50, Thermo Fisher Scientific), and collected on Superfrost plus slides (Thermo Fisher Scientific).

Tissue sections were rehydrated in PBS and blocked in 5% normal goat serum in PBS with 0.1% Triton X-100. Antigen retrieval was performed on sections being stained for OMP by steaming tissue for 45 min in citrate-based antigen unmasking solution (Vector Laboratories, Newark, CA). Anti–tubulin β3 (BioLegend, clone TUJ1, catalog no. 801201, AB_2313773; 1:500), anti-CD45 (BioLegend, clone HI30, catalog no. 304001, AB_314389; 1:50), anti-CD3 (BioLegend, clone HIT3a, catalog no. 300301; AB_314037; 1:50), anti-CD68 (BioLegend, clone BL13756, catalog no. 375602, AB_2876705; 1:50), anti-CD207 (Langerin) (BioLegend, clone 4C7, catalog no. 144201, AB_2562087; 1:50), anti–TCR γ/δ (BioLegend, clone B1, catalog no. 331202, AB_1089222; 1:50), anti-ERMN (Thermo Fisher Scientific, catalog no. PA5-58327, AB_264 1113; 1:100), anti–SARS-CoV-2 nucleocapsid (Novus, NB100-56576, AB_838838; 1:250), anti-SOX2 (Invitrogen eBioscience, catalog no. 14-9811-82, AB_11219471; 1:50), or anti-OMP (Santa Cruz Biotechnology, catalog no. sc-365818, AB_10842164; 1:500) primary antibodies diluted in blocking buffer were incubated on tissue sections for 1 hour at room temperature or overnight at 4°C. After PBS washes, tissues were incubated with fluorescence-conjugated secondary antibodies for 45 min (Jackson ImmunoResearch, West Grove, PA). Vectashield with 4′,6-diamidino-2-phenylindole (DAPI) (Vector Laboratories, Burlingame, CA) was applied to each section before coverslipping. All images were acquired on a Leica DMi8 microscope system (Leica Microsystems). Images were analyzed using ImageJ software (v.2.3.0), and scale bars were applied using metadata from the original Leica acquisition software files.

For quantification of immunohistochemical labeling, Images were acquired with 40× objective and opened in ImageJ. Staining of adjacent sections with TUJ1/ERMN confirmed the presence of olfactory epithelium rather than respiratory epithelium. Counts were conducted across a minimum of 500-μm length of olfactory epithelium (average length counted per patient = 931 μm). Olfactory sensory neurons were counted on the basis of the presence of an $OMP^+$ cell soma and dendrite with associated $DAPI^+$ nucleus. Sustentacular cells were counted on the basis of $SOX2^+$ nuclei. Only apical $SOX2^+$ nuclei were counted as sustentacular cells, excluding $SOX2^+$ horizontal basal cells, distinctly situated against the basement membrane with small flat morphology. For each patient, the total ratio of $OMP^+$ cells to total $SOX2^+$ apical cells was calculated. Adjacent sections were not included in counts for a given cell type–specific marker, avoiding a need for using Abercrombie correction.

### Olfactory mucus assays

Mucus was obtained from the olfactory cleft using absorbent filter paper under endoscopic guidance per an approved IRB protocol at UC San Diego (#210078). Cohorts included PASC hyposmics ($n$ = 13 patients) or control normosmics ($n$ = 7), based on psychophysical testing using the Smell Identification Test. A fluorescent bead-based multiplex assay (LegendPlex, BioLegend) was used to quantify 13 cytokines/chemokines via flow cytometry.

### Statistics

All sequencing dataset analyses were performed in Python or R using the toolkits and packages described above. Plots were produced using Scanpy, Matplotlib, ggplot2 in associated R toolkits (*48*), or GraphPad Prism 9. Cell phenotype comparisons between PASC hyposmic and control samples were performed using unpaired two-tailed $t$ test, with significance defined as $P < 0.05$. For all parametric tests, Shapiro-Wilk tests were used to assess normal distributions; appropriate significance tests were then used (either $t$ test or Mann-Whitney test). Differentially expressed genes were analyzed using Wilcoxon rank sum test. Error bars represent SEM. Differentially expressed gene sets were analyzed for gene ontology, cellular pathway, or tissue output terms using ToppGene Suite (*49*). Immunohistochemistry quantification was compared using one-way ANOVA with Tukey test, Bonferroni correction.

## Supplementary Materials

**This PDF file includes:**
Tables S1 and S2
Figs. S1 to S11

**Other Supplementary Material for this manuscript includes the following:**
Data file S1
MDAR Reproducibility Checklist

View/request a protocol for this paper from *Bio-protocol*.

## References and Notes


1. A. Carfì, R. Bernabei, F. Landi; Gemelli Against COVID-19 Post-Acute Care Study Group, Persistent symptoms in patients after acute COVID-19. *JAMA* **324**, 603–605 (2020).
2. S. E. Schambeck, C. S. Crowell, K. I. Wagner, E. D'Ippolito, T. Burrell, H. Mijočević, U. Protzer, D. H. Busch, M. Gerhard, H. Poppert, H. Beyer, Phantosmia, parosmia, and dysgeusia are prolonged and late-onset symptoms of COVID-19. *J. Clin. Med.* **10**, 5266 (2021).
3. K. Karamali, M. Elliott, C. Hopkins, COVID-19 related olfactory dysfunction. *Curr. Opin. Otolaryngol. Head Neck Surg.* **30**, 19–25 (2022).
4. P. Boscolo-Rizzo, T. Hummel, C. Hopkins, M. Dibattista, A. Menini, G. Spinato, C. Fabbris, E. Emanuelli, A. D'Alessandro, R. Marzolino, E. Zanelli, E. Cancellieri, K. Cargnelutti, S. Fadda, D. Borsetto, L. A. Vaira, N. Gardenal, J. Polesel, G. Tirelli, High prevalence of long-term olfactory, gustatory, and chemesthesis dysfunction in post-COVID-19 patients: A matched case-control study with one-year follow-up using a comprehensive psychophysical evaluation. *Rhinology* **59**, 517–527 (2021).
5. P. Boscolo-Rizzo, A. Menegaldo, C. Fabbris, G. Spinato, D. Borsetto, L. A. Vaira, L. Calvanese, A. Pettorelli, M. Sonego, D. Frezza, A. Bertolin, W. Cestaro, R. Rigoli, A. D'Alessandro, G. Tirelli, M. C. Da Mosto, A. Menini, J. Polesel, C. Hopkins, Six-month psychophysical evaluation of olfactory dysfunction in patients with COVID-19. *Chem. Senses* **46**, bjab006 (2021).
6. G. A. Graziadei, P. P. Graziadei, Neurogenesis and neuron regeneration in the olfactory system of mammals. II. Degeneration and reconstitution of the olfactory sensory neurons after axotomy. *J. Neurocytol.* **8**, 197–213 (1979).
7. C. T. Leung, P. A. Coulombe, R. R. Reed, Contribution of olfactory neural stem cells to tissue maintenance and regeneration. *Nat. Neurosci.* **10**, 720–726 (2007).
8. J. E. Schwob, W. Jang, E. H. Holbrook, B. Lin, D. B. Herrick, J. N. Peterson, J. Hewitt Coleman, Stem and progenitor cells of the mammalian olfactory epithelium: Taking poietic license. *J. Comp. Neurol.* **525**, 1034–1054 (2017).
9. M. A. Durante, S. Kurtenbach, Z. B. Sargi, J. W. Harbour, R. Choi, S. Kurtenbach, G. M. Goss, H. Matsunami, B. J. Goldstein, Single-cell analysis of olfactory neurogenesis and differentiation in adult humans. *Nat. Neurosci.* **23**, 323–326 (2020).
10. R. Choi, B. J. Goldstein, Olfactory epithelium: Cells, clinical disorders, and insights from an adult stem cell niche. *Laryngoscope Investig. Otolaryngol.* **3**, 35–42 (2018).
11. L. Buck, R. Axel, A novel multigene family may encode odorant receptors: A molecular basis for odor recognition. *Cell* **65**, 175–187 (1991).
12. M. Zazhytska, A. Kodra, D. A. Hoagland, J. Frere, J. F. Fullard, H. Shayya, N. G. McArthur, R. Moeller, S. Uhl, A. D. Omer, M. E. Gottesman, S. Firestein, Q. Gong, P. D. Canoll, J. E. Goldman, P. Roussos, B. R. tenOever, J. B. Overdevest, S. Lomvardas, Non-cell-autonomous disruption of nuclear architecture as a potential cause of COVID-19-induced anosmia. *Cell* **185**, 1052–1064.e12 (2022).
13. D. H. Brann, T. Tsukahara, C. Weinreb, M. Lipovsek, K. Van den Berge, B. Gong, R. Chance, I. C. Macaulay, H.-J. Chou, R. B. Fletcher, D. Das, K. Street, H. R. de Bezieux, Y.-G. Choi, D. Risso, S. Dudoit, E. Purdom, J. Mill, R. A. Hachem, H. Matsunami, D. W. Logan, B. J. Goldstein, M. S. Grubb, J. Ngai, S. R. Datta, Non-neuronal expression of SARS-CoV-2 entry genes in the olfactory system suggests mechanisms underlying COVID-19-associated anosmia. *Sci. Adv.* **6**, eabc5801 (2020).
14. B. Bryche, A. St Albin, S. Murri, S. Lacote, C. Pulido, M. Ar Gouilh, S. Lesellier, A. Servat, M. Wasniewski, E. Picard-Meyer, E. Monchatre-Leroy, R. Volmer, O. Rampin, R. Le Goffic, P. Marianneau, N. Meunier, Massive transient damage of the olfactory epithelium associated with infection of sustentacular cells by SARS-CoV-2 in golden Syrian hamsters. *Brain Behav. Immun.* **89**, 579–586 (2020).
15. J. F. Shelton, A. J. Shastri, K. Fletez-Brant; 23andMe COVID-19 Team, S. Aslibekyan, A. Auton, The UGT2A1/UGT2A2 locus is associated with COVID-19-related loss of smell or taste. *Nat. Genet.* **54**, 121–124 (2022).
16. M. Khan, S. J. Yoo, M. Clijsters, W. Backaert, A. Vanstapel, K. Speleman, C. Lietaer, S. Choi, T. D. Hether, L. Marcelis, A. Nam, L. Pan, J. W. Reeves, P. Van Bulck, H. Zhou, M. Bourgeois, Y. Debaveye, P. De Munter, J. Gunst, M. Jorissen, K. Lagrou, N. Lorent, A. Neyrinck, M. Peetermans, D. R. Thal, C. Vandenbriele, J. Wauters, P. Mombaerts, L. Van Gerven, Visualizing in deceased COVID-19 patients how SARS-CoV-2 attacks the respiratory and olfactory mucosae but spares the olfactory bulb. *Cell* **184**, 5932–5949.e15 (2021).
17. R. L. Doty, P. Shaman, M. Dann, Development of the University of Pennsylvania Smell Identification Test: A standardized microencapsulated test of olfactory function. *Physiol. Behav.* **32**, 489–502 (1984).
18. R. L. Doty, P. Shaman, S. L. Applebaum, R. Giberson, L. Siksorski, L. Rosenberg, Smell identification ability: Changes with age. *Science* **226**, 1441–1443 (1984).
19. A. D. Oliva, R. Gupta, K. Issa, R. Abi Hachem, D. W. Jang, S. A. Wellford, E. A. Moseman, H. Matsunami, B. J. Goldstein, Aging-related olfactory loss is associated with olfactory stem cell transcriptional alterations in humans. *J. Clin. Invest.* **132**, e155506 (2022).
20. C. Gutmann, K. Takov, S. A. Burnap, B. Singh, H. Ali, K. Theofilatos, E. Reed, M. Hasman, A. Nabeebaccus, M. Fish, M. J. McPhail, K. O'Gallagher, L. E. Schmidt, C. Cassel, M. Rienks, X. Yin, G. Auzinger, S. Napoli, S. F. Mujib, F. Trovato, B. Sanderson, B. Merrick, U. Niazi, M. Saqi, K. Dimitrakopoulou, R. Fernández-Leiro, S. Braun, R. Kronstein-Wiedemann, K. J. Doores, J. D. Edgeworth, A. M. Shah, S. R. Bornstein, T. Tonn, A. C. Hayday, M. Giacca, M. Shankar-Hari, M. Mayr, SARS-CoV-2 RNAemia and proteomic trajectories inform prognostication in COVID-19 patients admitted to intensive care. *Nat. Commun.* **12**, 3406 (2021).
21. J. J. Frere, R. A. Serafini, K. D. Pryce, M. Zazhytska, K. Oishi, I. Golynker, M. Panis, J. Zimering, S. Horiuchi, D. A. Hoagland, R. Møller, A. Ruiz, A. Kodra, J. B. Overdevest, P. D. Canoll, A. C. Borczuk, V. Chandar, Y. Bram, R. Schwartz, S. Lomvardas, V. Zachariou, B. R. tenOever, SARS-CoV-2 infection in hamsters and humans results in lasting and unique systemic perturbations post recovery. *Sci. Transl. Med.* **7**, eabq3059 (2022).
22. P. A. Szabo, H. M. Levitin, M. Miron, M. E. Snyder, T. Senda, J. Yuan, Y. L. Cheng, E. C. Bush, P. Dogra, P. Thapa, D. L. Farber, P. A. Sims, Single-cell transcriptomics of human T cells reveals tissue and activation signatures in health and disease. *Nat. Commun.* **10**, 4706 (2019).
23. G. Pizzolato, H. Kaminski, M. Tosolini, D. M. Franchini, F. Pont, F. Martins, C. Valle, D. Labourdette, S. Cadot, A. Quillet-Mary, M. Poupot, C. Laurent, L. Ysebaert, S. Meraviglia, F. Dieli, P. Merville, P. Milpied, J. Dechanet-Merville, J.-J. Fournie, Single-cell RNA sequencing unveils the shared and the distinct cytotoxic hallmarks of human TCRVδ1 and TCRVδ2 γδ T lymphocytes. *Proc. Natl. Acad. Sci. U.S.A.* **116**, 11906–11915 (2019).
24. M. Bonneville, R. L. O'Brien, W. K. Born, Gammadelta T cell effector functions: A blend of innate programming and acquired plasticity. *Nat. Rev. Immunol.* **10**, 467–478 (2010).
25. G. von Massow, S. Oh, A. Lam, K. Gustafsson, Gamma delta T cells and their involvement in COVID-19 virus infections. *Front. Immunol.* **12**, 741218 (2021).

26. C. E. Allen, M. Merad, K. L. McClain, Langerhans-cell histiocytosis. *N. Engl. J. Med.* **379**, 856–868 (2018).
27. M. Merad, F. Ginhoux, M. Collin, Origin, homeostasis and function of Langerhans cells and other langerin-expressing dendritic cells. *Nat. Rev. Immunol.* **8**, 935–947 (2008).
28. S. M. Lee, K. H. Kok, M. Jaume, T. K. Cheung, T. F. Yip, J. C. Lai, Y. Guan, R. G. Webster, D. Y. Jin, J. S. Peiris, Toll-like receptor 10 is involved in induction of innate immune responses to influenza virus infection. *Proc. Natl. Acad. Sci. U.S.A.* **111**, 3793–3798 (2014).
29. Y. K. Alshoubaki, B. Nayer, S. Das, M. M. Martino, Modulation of the activity of stem and progenitor cells by immune cells. *Stem Cells Transl. Med.* **11**, 248–258 (2022).
30. R. Ueha, K. Kondo, S. Ueha, T. Yamasoba, Dose-dependent effects of insulin-like growth factor 1 in the aged olfactory epithelium. *Front. Aging Neurosci.* **10**, 385 (2018).
31. Y. Chen, M. L. Getchell, X. Ding, T. V. Getchell, Immunolocalization of two cytochrome P450 isozymes in rat nasal chemosensory tissue. *Neuroreport* **3**, 749–752 (1992).
32. D. B. Herrick, B. Lin, J. Peterson, N. Schnittke, J. E. Schwob, Notch1 maintains dormancy of olfactory horizontal basal cells, a reserve neural stem cell. *Proc. Natl. Acad. Sci. U.S.A.* **114**, E5589–E5598 (2017).
33. W. D. Mahauad-Fernandez, C. M. Okeoma, The role of BST-2/Tetherin in host protection and disease manifestation. *Immun. Inflamm. Dis.* **4**, 4–23 (2016).
34. R. A. Liberatore, P. D. Bieniasz, Tetherin is a key effector of the antiretroviral activity of type I interferon in vitro and in vivo. *Proc. Natl. Acad. Sci. U.S.A.* **108**, 18097–18101 (2011).
35. M. Chen, R. R. Reed, A. P. Lane, Chronic inflammation directs an olfactory stem cell functional switch from neuroregeneration to immune defense. *Cell Stem Cell* **25**, 501–513.e5 (2019).
36. A. Keller, F. L. Margolis, Immunological studies of the rat olfactory marker protein. *J. Neurochem.* **24**, 1101–1106 (1975).
37. T. Olender, I. Keydar, J. M. Pinto, P. Tatarskyy, A. Alkelai, M.-S. Chien, S. Fishilevich, D. Restrepo, H. Matsunami, Y. Gilad, D. Lancet, The human olfactory transcriptome. *BMC Genomics* **17**, 619 (2016).
38. M. Fitzek, P. K. Patel, P. D. Solomon, B. Lin, T. Hummel, J. E. Schwob, E. H. Holbrook, Integrated age-related immunohistological changes occur in human olfactory epithelium and olfactory bulb. *J. Comp. Neurol.* **530**, 2154–2175.
39. A. Nalbandian, K. Sehgal, A. Gupta, M. V. Madhavan, C. McGroder, J. S. Stevens, J. R. Cook, A. S. Nordvig, D. Shalev, T. S. Sehrawat, N. Ahluwalia, B. Bikdeli, D. Dietz, C. Der-Nigoghossian, N. Liyanage-Don, G. F. Rosner, E. J. Bernstein, S. Mohan, A. A. Beckley, D. S. Seres, T. K. Choueiri, N. Uriel, J. C. Ausiello, D. Accili, D. E. Freedberg, M. Baldwin, A. Schwartz, D. Brodie, C. K. Garcia, M. S. V. Elkind, J. M. Connors, J. P. Bilezikian, D. W. Landry, E. Y. Wan, Post-acute COVID-19 syndrome. *Nat. Med.* **27**, 601–615 (2021).
40. S. Havervall, A. Rosell, M. Phillipson, S. M. Mangsbo, P. Nilsson, S. Hober, C. Thålin, Symptoms and functional impairment assessed 8 months after mild COVID-19 among health care workers. *JAMA* **325**, 2015–2016 (2021).
41. S. Bohnacker, F. Hartung, F. Henkel, A. Quaranta, J. Kolmert, A. Priller, M. Ud-Dean, J. Giglberger, L. M. Kugler, L. Pechtold, S. Yazici, A. Lechner, J. Erber, U. Protzer, P. Lingor, P. Knolle, A. M. Chaker, C. B. Schmidt-Weber, C. E. Wheelock, J. E.-v. Bieren, Mild COVID-19 imprints a long-term inflammatory eicosanoid- and chemokine memory in monocyte-derived macrophages. *Mucosal Immunol.* **15**, 798 (2022).
42. Y. Su, D. Yuan, D. G. Chen, R. H. Ng, K. Wang, J. Choi, S. Li, S. Hong, R. Zhang, J. Xie, S. A. Kornilov, K. Scherler, A. J. Pavlovitch-Bedzyk, S. Dong, C. Lausted, I. Lee, S. Fallen, C. L. Dai, P. Baloni, B. Smith, V. R. Duvvuri, K. G. Anderson, J. Li, F. Yang, C. J. Duncombe, D. J. McCulloch, C. Rostomily, P. Troisch, J. Zhou, S. Mackay, Q. De Gottardi, D. H. May, R. Taniguchi, R. M. Gittelman, M. Klinger, T. M. Snyder, R. Roper, G. Wojciechowska, K. Murray, R. Edmark, S. Evans, L. Jones, Y. Zhou, L. Rowen, R. Liu, W. Chour, H. A. Algren, W. R. Berrington, J. A. Wallick, R. A. Cochran, M. E. Micikas; ISB-Swedish COVID-19 Biobanking Unit, T. Wrin, C. J. Petropoulos, H. R. Cole, T. D. Fischer, W. Wei, D. S. B. Hoon, N. D. Price, N. Subramanian, J. A. Hill, J. Hadlock, A. T. Magis, A. Ribas, L. L. Lanier, S. D. Boyd, J. A. Bluestone, H. Chu, L. Hood, R. Gottardo, P. D. Greenberg, M. M. Davis, J. D. Goldman, J. R. Heath, Multiple early factors anticipate post-acute COVID-19 sequelae. *Cell* **185**, 881–895 e20 (2022).
43. G. D. de Melo, F. Lazarini, S. Levallois, C. Hautefort, V. Michel, F. Larrous, B. Verillaud, C. Aparicio, S. Wagner, G. Gheusi, L. Kergoat, E. Kornobis, F. Donati, T. Cokelaer, R. Hervochon, Y. Madec, E. Roze, D. Salmon, H. Bourhy, M. Lecuit, P. M. Lledo, COVID-19-related anosmia is associated with viral persistence and inflammation in human olfactory epithelium and brain infection in hamsters. *Sci. Transl. Med.* **13**, eabf8396 (2021).
44. G. Douaud, S. Lee, F. Alfaro-Almagro, C. Arthofer, C. Wang, P. McCarthy, F. Lange, J. L. R. Andersson, L. Griffanti, E. Duff, S. Jbabdi, B. Taschler, P. Keating, A. M. Winkler, R. Collins, P. M. Matthews, N. Allen, K. L. Miller, T. E. Nichols, S. M. Smith, SARS-CoV-2 is associated with changes in brain structure in UK Biobank. *Nature* **604**, 697–707 (2022).
45. L. Zhang, A. Richards, M. I. Barrasa, S. H. Hughes, R. A. Young, R. Jaenisch, Reverse-transcribed SARS-CoV-2 RNA can integrate into the genome of cultured human cells and can be expressed in patient-derived tissues. *Proc. Natl. Acad. Sci. U.S.A.* **118**, e2105968118 (2021).
46. A. Butler, P. Hoffman, P. Smibert, E. Papalexi, R. Satija, Integrating single-cell transcriptomic data across different conditions, technologies, and species. *Nat. Biotechnol.* **36**, 411–420 (2018).
47. R. Browaeys, W. Saelens, Y. Saeys, NicheNet: Modeling intercellular communication by linking ligands to target genes. *Nat. Methods* **17**, 159–162 (2020).
48. H. Wickham, *ggplot2: Elegant Graphics for Data Analysis*. (Springer-Verlag, 2016).
49. J. Chen, E. E. Bardes, B. J. Aronow, A. G. Jegga, ToppGene suite for gene list enrichment analysis and candidate gene prioritization. *Nucleic Acids Res.* **37**, W305–W311 (2009).


**Acknowledgments:** We thank the patients who generously agreed to provide biopsy samples for this research. We appreciate the expert technical assistance of the Duke Molecular Genomics Core and bioinformatics assistance from V. Jain. We also thank clinical research coordinators A. Walker and V. Eifert for expert assistance. Graphical schematics were created with Biorender.com. **Funding:** This study was supported by NIH grants DC018371, DC016859 (B.J.G.), AG074324 (E.A.M.), and DC019956 (C.H.Y.) and by funding from the Duke Department of Head and Neck Surgery & Communication Sciences. **Author contributions:** B.J.G. designed the study and interpreted the data. D.W.J., R.A.-H., and B.J.G. obtained biopsy samples. J.B.F., A.D.O., T.K., and B.J.G. performed scRNA-seq experiments. C.H.Y. performed mucus assays and analysis. B.J.G., J.B.F., S.R.D., D.H.B., and T.T. analyzed scRNA-seq data. S.A.W., H.M., and E.A.M. provided resources and assisted in experimental design and interpretation. R.G. and J.B.F. performed immunostaining and analysis. J.B.F., B.J.G., D.H.B., T.T., and S.R.D. wrote the manuscript with input from all authors. **Competing interests:** B.J.G. has received consultancy fees from Frequency Therapeutics and discloses unpaid consulting for Rhino Therapeutics. D.W.J. has received research support from Medtronic and Association for Migraine Disorders. H.M. has received royalties from Chemcom, research grants from Givaudan, and consultant fees from Kao. **Data and materials availability:** scRNA-seq datasets are deposited in GEO with accession number GSE201620. Code availability: Scripts involved in analysis are available in Zenodo (DOI 10.5281/zenodo.7102415) at https://zenodo.org/record/7102415#.YyuFTiHMLao. 

Submitted 18 May 2022
Resubmitted 28 July 2022
Accepted 4 November 2022
Published 21 December 2022
10.1126/scitranslmed.add0484

Science Translational Medicine

# Persistent post–COVID-19 smell loss is associated with immune cell infiltration and altered gene expression in olfactory epithelium

John B. Finlay, David H. Brann, Ralph Abi Hachem, David W. Jang, Allison D. Oliva, Tiffany Ko, Rupali Gupta, Sebastian A. Wellford, E. Ashley Moseman, Sophie S. Jang, Carol H. Yan, Hiroaki Matsunami, Tatsuya Tsukahara, Sandeep Robert Datta, and Bradley J. Goldstein

*Sci. Transl. Med.*, **14** (676), eadd0484.
DOI: 10.1126/scitranslmed.add0484